Available online at www.sciencedirect.com
SCIENCE DIRECT
Biochemical and Biophysical Research Communications 343 (2006) 110–116
BBRC
www.elsevier.com/locate/ybbrc

Transient stability of the helical pattern of region F19–L22 of the N-terminal domain of p53: A molecular dynamics simulation study

L. Michel Espinoza-Fonseca [a,b,c,*], José G. Trujillo-Ferrara [b,c]

[a] *Department of Biochemistry, Molecular Biology and Biophysics, University of Minnesota, Minneapolis, MN 55455, USA*
[b] *Sección de Estudios de Posgrado e Investigación, Escuela Superior de Medicina del Instituto Politécnico Nacional, Apartado Postal 42-161, C.P. 11340, Mexico City, Mexico*
[c] *Departamento de Bioquímica, Escuela Superior de Medicina del Instituto Politécnico Nacional, Apartado Postal 42-161, C.P. 11340, Mexico City, Mexico*

Received 15 February 2006
Available online 3 March 2006

Abstract

Two molecular dynamics simulations of the region E17–N29 of p53 ($p53_{17–29}$) at different temperatures were performed for a total time of 0.2 μs, to study the conformational landscape of this region. Previous studies have suggested that this region displays different structural motifs, such as helix of a double β-turn, and that its secondary structure might be transiently stable. Interestingly, in this study it was found that the region F19–L25, and particularly its fragment F19–L22, display a stable, transient helical pattern at sub-microsecond periods. The region F19–L22, which contains one of the most important residues needed for the interaction of p53 with MDM2, seems to be formed and stabilized by the existence of one hydrophobic and one aromatic cluster. The main function of these clusters is to help their surrounding area to desolvate, to allow the hydrogen bond network, therefore favoring the formation of a stable helix. This preliminary study would be useful for a better understanding of the structure and function of the N-terminal domain of p53 and its implications for the control of different types of cancer.

Keywords: p53; N-terminal domain; Molecular dynamics simulations; Folding; p53–MDM2 interaction

p53, called by Lane as the "guardian of the genome" [1] and by Levine as a "cellular gatekeeper" [2], plays a central role in maintaining the genomic integrity of the cells. Its activation due to cellular stress induces cell-cycle arrest and apoptosis [3–5]. The structure of p53 contains a transcription activation domain and proline-rich region, which together constitute the N-terminal domain of the protein [6,7]. This region is followed by the DNA-binding domain [8], which is highly conserved, and a tetramerization domain [9,10]. Finally, a sequence-unspecific DNA-binding regulatory domain is found at the C-terminal domain of p53 [11,12].

Given the complexity of p53, its structure and function are still not well understood. Up to now, only the structures of the DNA-binding domain and the tetramerization domain have been solved by means of X-ray crystallography and NMR studies [13–17].

Unfortunately, few studies addressing the structure and function of the N-terminal domain of p53 have been published [18–20]. It has been shown that this region is natively unstructured, as demonstrated by NMR studies. However, it has been hypothesized that short regions transiently display an ordered behavior (e.g., they display well-defined secondary structure motifs) [21]. Particular interest has been paid to the region that binds MDM2, a protein that regulates p53 in an auto-regulatory feedback-loop [22]. MDM2 binds to the region T18–N29 of the N-terminal domain of p53, but only few residues play a key role in the molecular recognition mechanism and stabilization of the complex. In addition, this region contains highly conserved residues such as F19 and W23.

* Corresponding author.
E-mail address: mef@ddt.biochem.umn.edu (L.M. Espinoza-Fonseca).

0006-291X/$ - see front matter © 2006 Published by Elsevier Inc.
doi:10.1016/j.bbrc.2006.02.129

It has been postulated that, upon binding to MDM2, the region F19–L25 of p53 adopts an induced coil-to-helical pattern [23]. This pattern seems to be common for natively unfolded regions, in which flexible, highly specific conformation of a low binding affinity changes into a more ordered structure which displays higher binding affinity [24,25]. However, in other study, it was shown that region T18–L26 of p53 natively folds into a helix [19].

Considering those findings, in this study we performed relatively long, all-atom molecular dynamics simulations of the fragment E17–N29 of p53 at two different temperatures. Molecular dynamics simulations currently represent a useful tool to capture sub-microsecond transitions in proteins and allow a better sampling of the conformational landscape of a given biomolecule.

By using molecular dynamics simulations, in this study it was found that the region comprising residues F19–L22 may natively display both unstructured and structured patterns. A mechanism in which this region is stabilized is presented, and some of its biological implications are discussed.

Materials and methods

Systems setup. The structure of the fragment E17–N29 of the N-terminal domain of p53 (denoted here as $p53_{17–29}$) was taken from the X-ray structure of the complex MDM2–p53 [23]. The peptide was capped with an acetyl group to the N-terminus and *N*-methylamide to the C-terminus, and embedded in a TIP3P water box with dimensions of 60 Å in each direction (6449 molecules of water). Finally, one sodium counterion was added to the system in order to obtain a total charge of zero. All atoms were described using the CHARMM27 forcefield [26].

Molecular dynamics protocol. Two simulations were performed using the program NAMD 2.6 [27]. The NPT ensemble was used, and periodic boundary conditions [28] were imposed on the systems. The nonbonded cutoff, switching distance, and nonbonded pair-list distance were set to 9, 8, and 10.5 Å, respectively. The electrostatic term was described by using the particle mesh Ewald algorithm [29,30]. The SHAKE algorithm for bonds to hydrogen atoms allowed a 2 fs time step [31]. Constant pressure and temperature on the system were maintained with an isotropic Langevin barostat and a Langevin thermostat. Five hundred steps of conjugate gradient algorithm first minimized each system with restraints to protein backbone, followed by 500 steps without restraints. The systems were slowly warmed up for 30 ps and equilibrated for 80 ps with lower restraints, finishing at no restraints and 298.15 and 400 K, respectively. Finally, the two simulations were continued for 150 ns (298.15 K) and 50 ns (400 K).

Analysis. Visual Molecular Dynamics (VMD) program was used for clustering, visualization, rendering, and analysis [32]. The program STRIDE [33], included in VMD, was used to analyze the evolution of the secondary structure of $p53_{17–29}$.

Results

Conformational evolution of $p53_{17–29}$ at 298.15 K

The structural evolution of $p53_{17–29}$ throughout the 150 ns of simulation at 298.15 was analyzed by the secondary structure changes and simple clustering based on the root-mean-square deviation (RMSD) and the radius of gyration (RGYR) of the Cα trace. On this basis, the RMSD and RGYR of the entire peptide were computed every 10 ps. The plots of the RGYR and RMSD are shown in Fig. 1A.

The plot of the RGYR (Fig. 1A, blue line) shows a relatively ordered structure of the fragment throughout the first 140 ns of simulation, which approximately represents the 94% of the total time of simulation. In the plot mentioned above was included the trace of the RGYR computed for the single structure of $p53_{17–29}$ obtained via crystallographic studies of its complex with MDM2 (red line), which is believed to be the stable helical-induced form of this fragment. It was observed that, during the first 78 ns of simulation, the average RGYR of $p53_{17–29}$ in this simulation remained below the value obtained for the X-ray structure of the peptide (7.33 Å). Moreover, the RGYR remaining within this period of time did not show any significant change. After this period of time, larger fluctuations of the RGYR were observed, due to the lost of the helical pattern (ordered) of residues W23–L25. The largest value of RGYR observed for this fragment constitutes an intermediate state between the helical motif of the region F19–L22 and the completely unstructured form of $p53_{17–29}$.

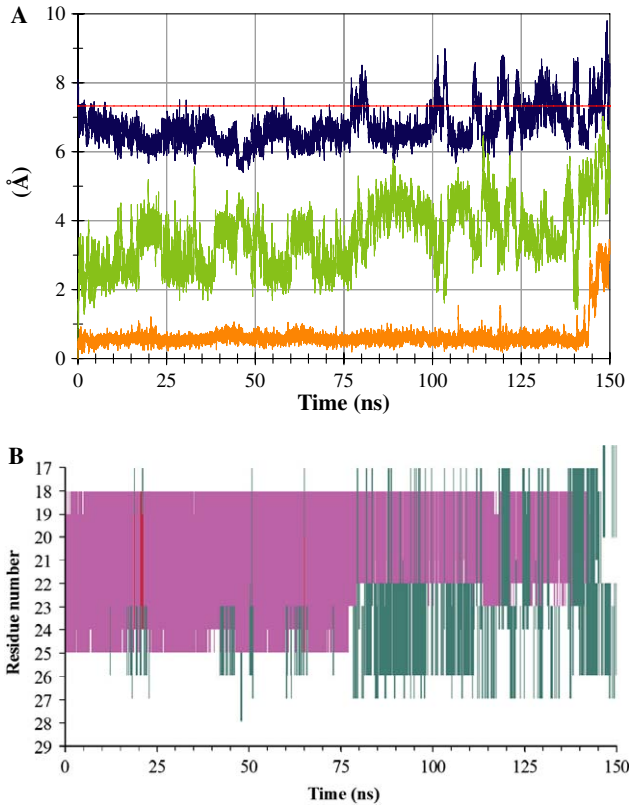

Fig. 1. (A) Radius of gyration (blue line), root-mean-square fluctuations of the full peptide (green line) and for the region F19–L22 of $p53_{17–29}$ (orange line) at 298.15 K. The red line represents the radius of gyration of $p53_{17–29}$ of the original X-ray structure. (B) Secondary structure of $p53_{17–29}$ throughout the 150-ns simulation. The secondary structure is colored as follows: purple, α-helix; red, π-helix; cyan, turn; white, random coil. (For interpretation of the references to color in this figure legend, the reader is referred to the web version of this paper.)

Similarly, when the RMSD is plotted for the entire fragment (Fig. 1A, green line), most of the values do not go beyond 5 Å in the first 78 ns, as observed for the fluctuations of the RGYR value in the same period of time. During the interval of time between 78 and 100 ns, $p53_{17–29}$ shows a drastic change on its RMSD, largely attributed to the loss of the ordered helical structure of residues W23–L25. After this period of time, the fluctuations of the RMSD of the fragment are significantly large, displaying in some cases a difference >4 Å. Since most of the large fluctuations of the RMSD come from the highly flexible termini of the peptide, the RMSD of the short region F19–L22N was calculated (Fig. 1A, orange line). It was observed that this fragment remains very stable until ~144 ns, displaying a RMSD <1 Å. After this period of time, a drastic increase of the RMSD was observed, reaching a maximum value of 3.3 Å.

To complement the plots described in the previous paragraphs, the secondary structure of individual residues of $p53_{17–29}$ was calculated every 10 ps (Fig. 1B). It was observed that the conformational fluctuations of the Cα trace represented by the RMSD and RGYR are in agreement with those of the secondary structure elements observed throughout the 150 ns of simulation. For instance, a stable helical pattern of the fragment F19–L25 was observed between 0 and 78 ns, while a very stable helical pattern observed for the fragment F19–L22 was obtained for more than 90% of the total simulation. Interestingly, transitions between the folded and unfolded structures of the fragment involve the formation of turns, as observed for the period of time between 138 and 145 ns.

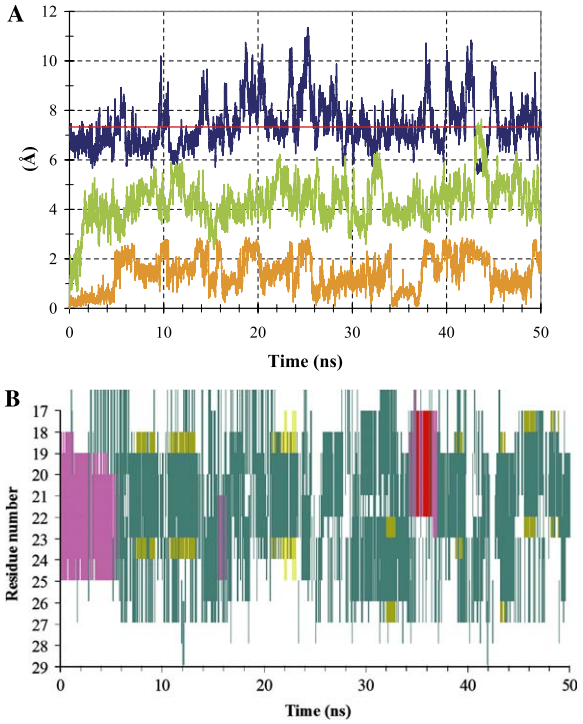

Fig. 2. (A) Radius of gyration (blue line), root-mean-square fluctuations of the full peptide (green line) and for the region F19–L22 of $p53_{17–29}$ (orange line) at 400 K. The red line represents the radius of gyration of $p53_{17–29}$ of the original X-ray structure. (B) Secondary structure of $p53_{17–29}$ throughout the 50-ns simulation at 400 K. The secondary structure is colored as follows: purple, α-helix; red, π-helix; yellow, β-sheet; green, isolated bridge; cyan, turn; white, random coil. (For interpretation of the references to color in this figure legend, the reader is referred to the web version of this paper.)

Conformational evolution of $p53_{17–29}$ at 400 K

In order to accelerate the conformational sampling of $p53_{17–29}$, a short MD simulation at 400 K was performed. To analyze the transitions and dynamics of the peptide over the time, the same analysis used for the simulation at 300 K was employed in this case. Thus, the RMSD and RGYR versus time were computed (Fig. 2A).

Given the high temperature of the simulation and the size of $p53_{17–29}$, large conformational transitions are expected. When the RGYR for individual snapshots over the time was plotted (Fig. 1A, blue line), changes ⩽1 Å on the values of RGYR were observed during the first 5 ns of simulation. After this period of time, large changes (RGYR > 2.5 Å) are observed. These changes are significantly larger compared to the value of RGYR calculated for the crystal structure of $p53_{17–29}$. Similarly, the plot of RMSD versus time (Fig. 2A, green line) shows a highly dynamic structure of peptide along the simulation. In this case, a stable structure of $p53_{17–29}$ was obtained during the first 2 ns of simulation. After this time, the peptide experienced long conformational changes (RMSD ⩾2 Å), leading to the formation of local structural motifs as well as completely unstructured regions.

Due to the high flexibility of the peptide at 400 K, the stability of its local structured regions was not easily distinguishable when the RGYR and RMSD values were analyzed. Considering that a high, local stability of the helical pattern of the region F19–L22 was observed in the 150-ns simulation at 298.15 K, the analysis of the RMSD was focused on this region. Thus, the values of RMSD were computed every 10 ps for the fragment F19–L22 (Fig. 2A, orange line). When the dynamics of this region was analyzed, some interesting features were observed. First, the helical pattern of this region remains constant during the first 4.5 ns, where the RMSD displayed a roughly constant RMSD value <1 Å. After this period of time, fluctuations larger than 1.5 Å were observed for the peptide along the 50 ns of simulation. Interestingly, when the RMSD of the helical pattern of this fragment (⩽0.5 Å) is compared to those obtained at different periods of time during the simulation, it was observed that, after the loss of the helical pattern of the fragment at ~5 ns, a very similar behavior was obtained at ~34.2 ns (Fig. 2A, orange line). This behavior remained constant for approximately 3 ns.

When the secondary structure motifs of individual residues of the peptide were analyzed over the 50 ns of simulation, it was confirmed that the helical pattern of the region

F19–L22 is regained between 34.2 and 37.2 ns (Fig. 2B). During this time, a very organized helical pattern of this 4-residue region was observed. The helical pattern contains not only α-helical motifs, but also few π-helical ones. This behavior might be attributed to the faster protein–protein and protein–water contacts, which increase the solvent accessibility of the peptide's backbone. After this period of time, the structure of the peptide returns to its unfolded state.

Throughout the simulation, other local secondary structure elements were observed, such as the formation of β-hairpins at 22 and 23 ns, and β-hairpin precursors at 7–14, 21, 32–33, 39–39.5, 43.5, 43.5–44.5, and 48 ns. The formation of these motifs might be intrinsic to the nature of the short peptide used in this study. However, it is possible that these intermediates do not exist in the folding pattern of the complete N-terminal domain of p53.

Discussion

The N-terminal domain of p53 has been believed to play an important role in the regulation of the p53 network. Unfortunately, the precise structure of this region and its biological implications have not been studied in depth. Thus, in this study, two independent molecular dynamics simulations of $p53_{17–29}$ were performed under different temperatures in order to largely explore the conformational transitions and dynamic stability of this region, obtaining a total of 0.2 μs of simulation. The analysis of the secondary structure of this peptide and its dynamical behavior suggests that the helical pattern of short regions of this fragment of p53 is found in its unbound form. In addition, this helical structure is found transiently, as suggested in a previous study [21].

We have found that, at room temperature, the structure of $p53_{17–29}$ remained almost unchanged during the ~78 ns of simulation. A similar observation was made when short regions of this peptide displayed a very stable helical pattern [19]. Particularly, the region comprising residues F19–L22 remained fairly constant for more than 140 ns, which is quite surprising for small peptides such as the one used in the present study. This region has been found to be conserved and its high content of hydrophobic residues seems to play an essential role in its regulation by MDM2. Given the limitations of the current molecular dynamics methodologies, we subjected $p53_{17–29}$ to a high-temperature molecular dynamics simulation in order to speed up the conformational sampling of the peptide in an aqueous environment. During the 50 ns of simulation, some very interesting features of this peptide were observed.

In first place, the helical pattern of the region F19–L25 does not remain stable for a relatively long period of time (less than 80 ns in our simulation at 298.15 K). However, a shorter region comprising residues F19–L22 keeps its helical motif for more than 100 ns, and is completely lost after ~140 ns. When we compared this behavior to that obtained at 400 K, a very interesting behavior was observed. As expected, the helical pattern of the region F19–L25 is lost after a short period of time (~5 ns). Afterwards, the peptide experienced several conformational changes, leading to the formation of other structural motifs such as β-hairpin precursors. Strikingly, a reestablishment of the helical pattern of the region F19–L22 was obtained for a period of time of ~3 ns (See Fig. 2B).

Buchner and co-workers have carried out some studies to determine the native conformation of the NTD of p53 [20,21]. In their studies, they found that most of the N-terminal domain is unstructured. However, they suggested that this region also contains folded, well-structured regions, and that these regions work synergistically with the unfolded regions [21]. In a NMR study performed by Han and co-workers, it was experimentally shown that the region T18–L26 of the full-length transcription activation domain of p53 displayed a strong helical pattern [19]. These authors also proposed that the presence of a "preexisting" helix instead of a coil-to-helix folding pattern would constitute the structural transition of the p53 transcription activation domain upon target binding, and that a tightening of the preexisting helix would lead to a stable helix. In contrast, a study performed by Chen and co-workers showed that the small fragment L14–E28 of p53 displayed two β-turns, which stabilized by a hydrophobic cluster consisting of residues known to be important for transcription/activation and binding to p53-binding proteins [18]. Even though these results are somehow contradictory, there is a high possibility that this region of the NTD of p53 will actually display diverse, unrelated conformations throughout the time. A possible explanation for this behavior will be discussed in the subsequent paragraphs.

To determine which regions of $p53_{17–29}$ play an important role in the formation of well-defined structural motifs, snapshots of the simulations at 298.15 (Fig. 3) and at 400 K (Fig. 4) representing the important conformational changes were taken and their structures analyzed. We focused our attention to residues F19 and W23, which are two important residues needed for the interaction between p53 and MDM2. These residues are surrounded by other hydrophobic residues, such as L22, L25, and L26. Considering the composition of this region and the information extracted from our simulations, a possible mechanism of stabilization/destabilization of this fragment is proposed as follows. The formation of the helical pattern of the region F19–L22 as well as the longer fragment F19–L25 is given due to the formation and stabilization of a hydrophobic cluster between residues F19, L22, and W23. In addition, the existence of an aromatic cluster between F19 and W23 was observed for ~140 ns of the simulation at 298.15 K as well as for the short helix obtained at ~34.2 ns in the 298.15 K simulation. Both hydrophobic and aromatic clusters seem to play a very important role in reestablishing the helical pattern of the small region F19–L22. It can be better observed in the snapshots taken from the simulation of $p53_{17–29}$ at 400 K (Fig. 4). In this

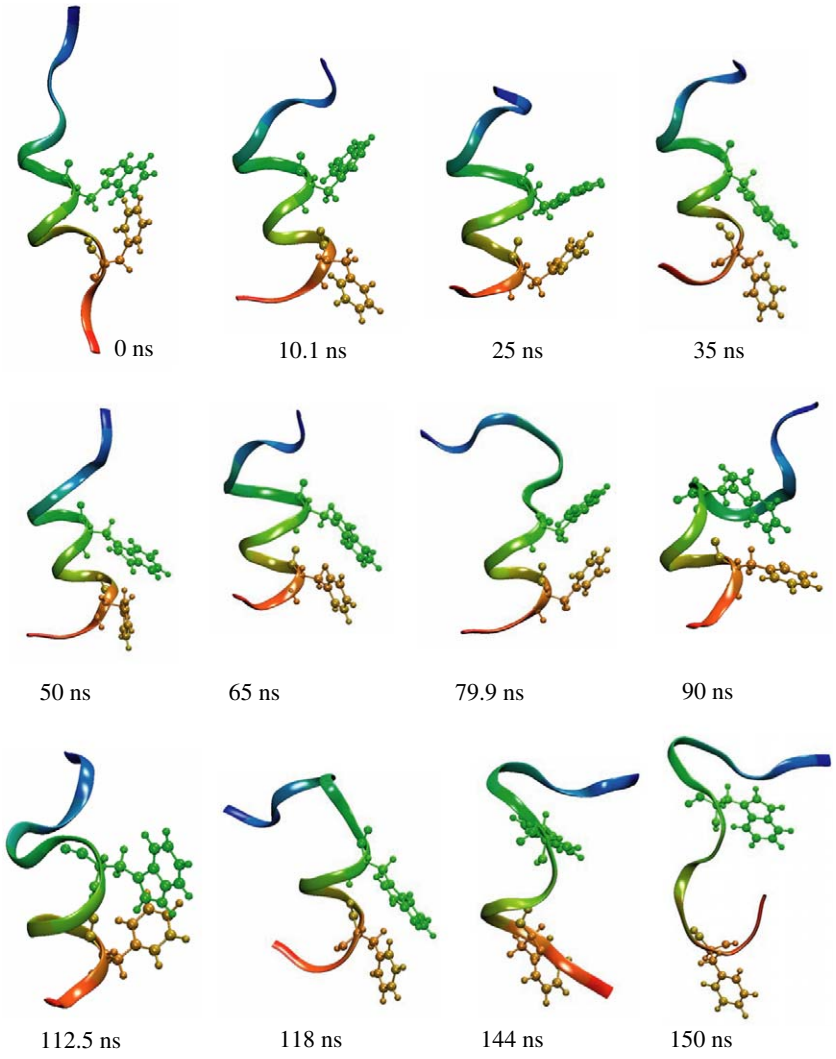

Fig. 3. Representative snapshots taken from the 150-ns simulation of $p53_{17–29}$. Residues F19 (brown) and W23 (green) are rendered as balls and sticks. (For interpretation of the references to color in this figure legend, the reader is referred to the web version of this paper.)

case, at ~34.2 ns, a helix precursor is obtained due to the formation of a hydrophobic cluster. This hydrophobic cluster is formed by residues F19, L22, and W23. The formation of this hydrophobic cluster favors the desolvation of the backbone of this region and the eventual formation of a short helix. In a second step, the stabilization of the helical pattern in the region F19–L22 is favored by the formation of an aromatic cluster between F19 and W23 (Fig. 4, 35.7 ns). In this case, "sandwich" and "T-shaped" π–π interactions govern most of the contacts between these two residues. Finally, a stable helical conformation is reached, and both hydrophobic and aromatic interactions work synergistically to stabilize it.

The destabilization/stabilization mechanism of the helical pattern of this region is still not clear, but it might be possible that some of the hydrophilic residues in this region such as S20 or D21 favor the solvation of the backbone, therefore considerably increasing the solvent-access surface area of the backbone and finally the disruption of the hydrogen bonding network of the helix.

It was mentioned that a NMR study of the fragment L14–E28 showed that a double β-turn pattern is obtained for this fragment [18]. When we analyzed the conformational changes of the peptide at 400 K, several turns were observed throughout the time, some of them at the regions reported by Han and co-workers. It is possible that in the studies mentioned above only few structural motifs of this region were observed. These contradictory observations could be explained due to the fact that the broad conformational landscape of the region was not fully sampled, and that only one energetic minimum was recorded in the NMR studies. Therefore, important conformational transitions such as helix precursors as well as other structural motifs that exist locally and transiently in this region would not be observed.

In summary, this preliminary study demonstrated that the region F19–L22 of p53 displays a stable, transient helical pattern. This fragment of p53 contains the most important residues involved in the molecular recognition mechanism by MDM2, a negative regulator of

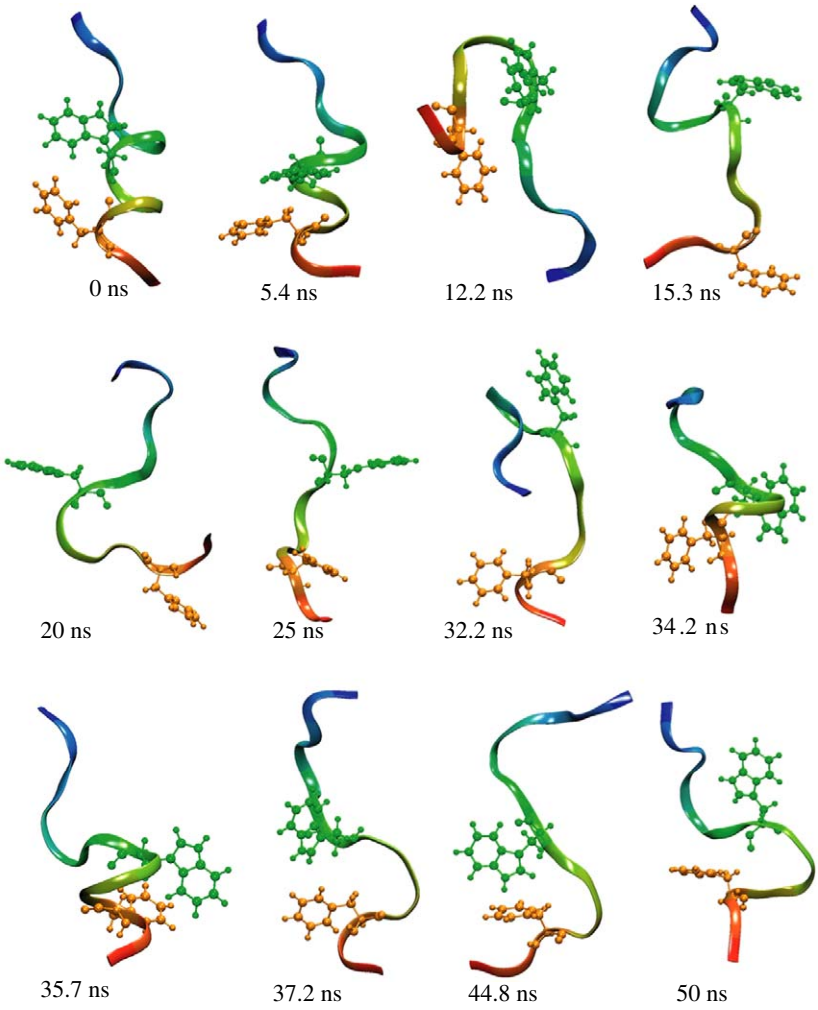

Fig. 4. Representative snapshots taken from the 50-ns simulation of $p53_{17–29}$. Residues F19 (brown) and W23 (green) are rendered as balls and sticks. (For interpretation of the references to color in this figure legend, the reader is referred to the web version of this paper.)

transcription [23,34–38]. The biological significance of the co-existence of transient structural motifs and unstructured regions has far-reaching consequences. A mostly unstructured region of the N-terminal domain of p53 might allow a great deal of promiscuity, needed to recognize a large number of molecules, and therefore modulate its transcription/activation functions. However, critical processes, such as the auto-regulatory feedback-loop one by MDM2, might require very specific recognition patterns that unstructured regions might lack. Therefore, the existence of transient, well-structured regions would give p53 the specificity needed to recognize some of its incoming partners.

It has been shown that the binding of MDM2 induces a helical pattern in the region F19–L25 of p53 [23]. However, the results obtained in this study suggest that the very short region F19–L22 of p53 might play a crucial role in the recognition mechanism between MDM2 and p53. Thus, this region might serve as an anchor between p53 and MDM2, leading to the formation of a more stable complex. Further questions arising from this study such as how specific is the interaction between p53 and MDM2, how the ratio between structured and unstructured populations is regulated, and how these regions work together need to be carefully weighted and addressed in future experimental and computational studies. Even though more work needs to be performed, this study will be helpful for a better understanding of the structure and function of the N-terminal domain of p53 and its implications for the control of different types of cancer.

Acknowledgments

L.M.E.F would like to thank David D. Thomas for his support and encouragement. The authors' research was supported by supercomputing time granted by the Minnesota Supercomputing Institute, University of Minnesota to L.M.E.F. and by grants from CONACYT and CGPI-IPN to J.G.T.F.

References

[1] D.P. Lane, Cancer. P53, guardian of the genome, Nature 358 (1992) 15–16.

[2] A.J. Levine, p53, the cellular gatekeeper for the growth and division, Cell 88 (1997) 323–331.
[3] M.B. Kastan, O. Onyekwere, D. Sidransky, B. Vogelstein, R.W. Craig, Participation of p53 protein in the cellular response to DNA damage, Cancer Res. 51 (1991) 6304–6311.
[4] X. Wu, A.J. Levine, p53 and E2F-1 cooperate to mediate apoptosis, Proc. Natl. Acad. Sci. USA 91 (1994) 3602–3606.
[5] H. Hermeking, D. Eick, Mediation of c-Myc-induced apoptosis by p53, Science 265 (1994) 2091–2093.
[6] S. Fields, S.K. Jang, Presence of a potent transcription activating sequence in the p53 protein, Science 249 (1990) 1046–1049.
[7] L. Raycroft, H.Y. Wu, G. Lozano, Transcriptional activation by wild-type but not transforming mutants of the p53 anti-oncogene, Science 249 (1990) 1049–1051.
[8] S.E. Kern, K.W. Kinzler, A. Bruskin, D. Jarosz, P. Friedman, C. Prives, B. Vogelstein, Identification of p53 as a sequence-specific DNA-binding protein, Science 252 (1991) 1708–1711.
[9] H.W. Sturzbecher, R. Brain, C. Addison, K. Rudge, M. Remm, M. Grimaldi, E. Keenan, J.R. Jenkins, A C-terminal alpha-helix plus basic region motif is the major structural determinant of p53 tetramerization, Oncogene 7 (1992) 1513–1523.
[10] K. Iwabuchi, B. Li, P. Bartel, S. Fields, Use of the two-hybrid system to identify the domain of p53 involved in oligomerization, Oncogene 8 (1993) 1693–1696.
[11] R.R. Rustandi, D.M. Baldisseri, D.J. Weber, Structure of the negative regulatory domain of p53 bound to S100B(ββ), Nat. Struct. Biol. 7 (2000) 570–574.
[12] J. Ahn, C. Prives, The C-terminus of p53: the more you learn the less you know, Nat. Struct. Biol. 8 (2001) 730–732.
[13] Y. Cho, S. Gorina, P.D. Jeffrey, N.P. Pavletich, Crystal structure of a p53 tumor suppressor-DNA complex: understanding tumorigenic mutations, Science 265 (1994) 346–355.
[14] W. Lee, T.S. Harvey, Y. Yin, P. Yau, D. Litchfield, C.H. Arrowsmith, Solution structure of the tetrameric minimum transforming domain of p53, Nat. Struct. Biol. 1 (1994) 877–890.
[15] J.S. Butler, S.N. Loh, Structure, function, and aggregation of the zinc-free form of the p53 DNA binding domain, Biochemistry 42 (2003) 2396–2403.
[16] P.D. Jeffrey, S. Gorina, N.P. Pavletich, Crystal structure of the tetramerization domain of the p53 tumor suppressor at 1.7 angstroms, Science 267 (1995) 1498–1502.
[17] S. Gorina, N.P. Pavletich, Structure of the p53 tumor suppressor bound to the ankyrin and SH3 domains of 53BP2, Science 274 (1996) 1001–1005.
[18] M.V. Botuyan, J. Momand, Y. Chen, Solution conformation of an essential region of the p53 transactivation domain, Fold. Des. 2 (1997) 331–342.
[19] H. Lee, K.H. Mok, R. Muhandiram, K.H. Park, J.E. Suk, D.H. Kim, J. Chang, Y.C. Sung, K.Y. Choi, K.H. Han, Local structural elements in the mostly unstructured transcriptional activation domain of human p53, J. Biol. Chem. 275 (2000) 29426–29432.
[20] S. Bell, C. Klein, L. Muller, S. Hansen, J. Buchner, p53 contains large unstructured regions in its native state, J. Mol. Biol. 322 (2002) 917–927.
[21] R. Dawson, L. Muller, A. Dehner, C. Klein, H. Kessler, J. Buchner, The N-terminal domain of p53 is natively unfolded, J. Mol. Biol. 332 (2003) 1131–1141.
[22] S.L. Harris, A.J. Levine, The p53 pathway: positive and negative feedback loops, Oncogene 24 (2005) 2899–2908.
[23] P.H. Kussie, S. Gorina, V. Marechal, B. Elenbaas, J. Moreau, A.J. Levine, N.P. Pavletich, Structure of the MDM2 oncoprotein bound to the p53 tumor suppressor transactivation domain, Science 274 (1996) 948–953.
[24] P. Tompa, Intrinsically unstructured proteins, Trends Biochem. Sci. 27 (2002) 527–533.
[25] A.K. Dunker, J.D. Lawson, C.J. Brown, R.M. Williams, P. Romero, J.S. Oh, C.J. Oldfield, A.M. Campen, C.M. Ratliff, K.W. Hipps, J. Ausio, M.S. Nissen, R. Reeves, C. Kang, C.R. Kissinger, R.W. Bailey, M.D. Griswold, W. Chiu, E.C. Garner, Z. Obradovic, Intrinsically disordered protein, J. Mol. Graph. Model. 19 (2001) 26–59.
[26] A.D. MacKerell Jr., D. Bashford, M. Bellott, R.L. Dunbrack Jr., J.D. Evanseck, M.J. Field, S. Fischer, J. Gao, H. Guo, S. Ha, D. Joseph-McCarthy, L. Kuchnir, K. Kuczera, F.T.K. Lau, C. Mattos, S. Michnick, T. Ngo, D.T. Nguyen, B. Prodhom, W.E. Reiher III, B. Roux, M. Schlenkrich, J.C. Smith, R. Stote, J. Straub, M. Watanabe, J. Wiorkiewicz-Kuczera, D. Yin, M. Karplus, All-atom empirical potential for molecular modeling and dynamics studies of proteins, J. Phys. Chem. B 102 (1998) 3586–3616.
[27] L. Kale, R. Skeel, M. Bhandarkar, R. Brunner, A. Gursoy, N. Krawetz, J. Phillips, A. Shinozaki, K. Varadarajan, K. Schulten, NAMD2: greater scalability for parallel molecular dynamics, J. Comput. Phys. 151 (1999) 283–312.
[28] W. Weber, P.H. Hünenberger, J.A. McCammon, Molecular dynamics simulations of a polyalanine octapeptide under Ewald boundary conditions: influence of artificial periodicity on peptide conformation, J. Phys. Chem. B 104 (2000) 3668–3675.
[29] U. Essmann, L. Perera, M.L. Berkowitz, A smooth particle mesh Ewald method, J. Chem. Phys. 103 (1995) 8577–8593.
[30] T. Darden, D. York, L. Pedersen, Particle mesh Ewald: an N·log(N) method for Ewald sums in large systems, J. Chem. Phys. 98 (1993) 10089–10092.
[31] W.F. van Gunsteren, H.J.C. Berendsen, Algorithms for macromolecular dynamics and constraint dynamics, Mol. Phys. 34 (1977) 1311–1327.
[32] W. Humphrey, A. Dalke, K. Schulten, VMD—visual molecular dynamics, J. Mol. Graph. 14 (1996) 33–38.
[33] D. Frishman, P. Argos, Knowledge-based protein secondary structure assignment, Proteins 23 (1995) 566–579.
[34] J. Chen, V. Marechal, A.J. Levine, Mapping of the p53 and mdm-2 interaction domains, Mol. Cell. Biol. 13 (1993) 4107–4114.
[35] S.M. Picksley, B. Vojtesek, A. Sparks, D.P. Lane, Immunochemical analysis of the interaction of p53 with MDM2;—fine mapping of the MDM2 binding site on p53 using synthetic peptides, Oncogene 9 (1994) 2523–2529.
[36] H. Zhong, H.A. Carlson, Computational studies and peptidomimetic design for the human p53–MDM2 complex, Proteins 58 (2005) 222–234.
[37] J. Lin, A.K. Teresky, A.J. Levine, Two critical hydrophobic amino acids in the N-terminal domain of the p53 protein are required for the gain of function phenotypes of human p53 mutants, Oncogene 10 (1995) 2387–2390.
[38] B. Ma, Y. Pan, K. Gunasekaran, O. Keskin, R.B. Venkataraghavan, A.J. Levine, R. Nussinov, The contribution of the Trp/Met/Phe residues to physical interactions of p53 with cellular proteins, Phys. Biol. 2 (2005) S56–S66.